Universidad de Concepción
Dirección de Postgrado
Facultad de Ingeniería - Programa de Magíster en Ciencias de la Ingeniería con Mención en Ingeniería Civil

Avalanchas en una fosa de socavación alrededor de un cilindro hincado en arena: Un mecanismo relevante de socavación

(Sand slides in a scour hole around a sediment-embedded cylinder: An important scour mechanism)

Tesis para optar al grado de Magíster en Ciencias de la Ingeniería con mención en Ingeniería Civil

JORGE IGNACIO SOTO SÁEZ
CONCEPCIÓN-CHILE
2018

Profesor Guía: Oscar Link Lazo
Dpto. de Ingeniería Civil, Facultad de Ingeniería
Universidad de Concepción

ABSTRACT

The aperiodic dynamically rich horseshoe vortex system at the base of a sediment-embedded cylinder in a turbulent boundary layer is the main agent of scour, dislodging and transporting sediment particles, and producing sand slides at the sides of the scour hole. While the sediment transport is linked to the enhanced bed shear stresses induced by the horseshoe vortices, the precise scour mechanisms are not fully understood. Physical scouring mechanisms are not included in scour-depth equations. Therefore, a conceptual framework linking the sediment dynamics at the intra scour hole scale with the macroscale properties of the flow is missing.

In this work, the sand slides developed in a scour hole around a cylinder in a sand bed were experimentally investigated. Experiments were conducted in a laboratory flume with constant discharge and clear-water conditions, with flow intensities - corresponding to the ratio between the section averaged flow velocity and the critical velocity for inception of sediment motion- equal to 0.68, 0.78, and 0.84, until advanced stages of scour. Sand slides were recorded in a non-intrusive manner during a representative segment of time with a frequency of 30 fps using a video camera placed within a plexiglass cylinder of 15 cm in diameter.

Through a Proper Orthogonal Decomposition of the image sequences, two types of sand slides were identified: Type I was a short and long advancing sand slide, while Type II was an elongated and short advancing sand slide. In time, sand slides occurred intermittently in an aperiodic manner resembling the behavior of the horseshoe vortex. The frequency of occurrence of sand slides decreased, and magnitude of sand slides increased with time. The product of frequency and magnitude, which expresses the rate of erosion caused by sand slides, decreased in time, evidencing a reduction of erosion towards equilibrium conditions. Interestingly, the sand slide Strouhal number correlated with the dimensionless flow work, W* needed to deepen the scour hole depth, Z* in a given amount, $\partial Z^*/\partial W^*$. Sand slides of Type I occurred for low values of $\partial Z^*/\partial W^*$, while sand slides of Type II occurred for high values of $\partial Z^*/\partial W^*$. Apart from the well-known sediment dislodging, rolling and sliding due to the enhanced bed shear stresses, our results show that sand slides are an important scour mechanism, contributing to produce about 60% to the scoured volume, and decrease to 40% when flow intensity was increased.

ACKNOWLEDGEMENTS

The financial support provided by the Comisión Nacional de Investigación, Científica y Tecnológica (CONICYT) through project Fondecyt Nr. 1150997: Bridge pier scour under flood waves.

The author thanks Dr. Oscar Link for his theoretical knowledge in scour topics, Mr. René Iribarren for his help to materialize the laboratory experimental series, and Dr. Wernher Brevis for his collaboration through analysis methods.

Finally, the author thanks the unconditional support of his family and friends.

CONTENTS

LIST OF TABLES

LIST OF FIGURES

CHAPTER 1. INTRODUCTION

1.1. Motivation

The scour problem represents the leading cause of bridge collapses worldwide (Brandimarte *et al.*, 2012), therefore, it is highly important for the design of bridges foundations. Most of the research to date focused on the formulation of scour-depth equations based on bulk fluid parameters, sediment characteristics, and geometry, rather than on the physical mechanisms of local scouring. A conceptual framework linking the sediment dynamics at the intra scour hole scale with the macroscale properties of the flow is completely missed.

A deeper understanding of the fundamental physics of the phenomena aims to the development of protection methods and accurate bridge design. Most of the technical solutions resides in protect the erodible bed more than reduce the effect of the scouring source. It is necessary to provide detailed structural and dynamic information of the process, especially for high Reynolds number. Numerical models have attempted to include the effects of sand slides on scouring, by means of a mass balance and limiting the bed slope to be a few degrees larger than the angle of repose of the sediment. However a physically based description within a numerical framework model still needs to be developed.

The horseshoe vortex system (HSV), a vortex which develops when the turbulent boundary layer encounters an obstacle attached to the same surface, e.g. a pile, is a flow structure which has been identified as the main agent of scour, dislodging and transporting sediment particles, and producing sand slides at the sides of the scour hole. While the sediment transport mechanisms are clearly linked to the enhanced bed shear stresses induced by the horseshoe vortices, the mechanism linking the horseshoe vortex behavior and sand slides are not fully understood. Sand slides have been scarcely studied in the past.

1.2. Hypothesis

The sand slides are a mechanism which contributes to transport an important volume of sediment in a low frequency aperiodic manner.

1.3. Objectives

1.3.1. General objective

To analyze the features of side slides produced inside a scour hole around a sediment-embedded cylinder, and their contribution to scouring processes through advanced measuring techniques at the laboratory scale.

1.3.2. Specific objectives

a) To perform laboratory scour experiments with constant discharge under clear water conditions to study the dynamics of side-slides.

b) To analyze the spatial and temporal patterns of side-slides in a scour hole.

c) To explore the correlation between the temporal and spatial sand slides features and the large bulk flow properties, such as the dimensionless flow work.

1.4. Methodology

A deep background review about the dynamic of the horseshoe vortex system on flat and scoured bed, as well as the effect of this complex system over the sediment was necessary to understand

the mechanism of sediment transport inside the scour hole. This defined the experimental setup and experimental series.

The scour measuring and sand slide recording system were chosen aiming that both systems were non-intrusive. Then, the scour depth, the sand slides occurrence and volume were measured. The analysis techniques were used to extract the main temporal and spatial features which were comparable with the behavior of the horseshoe vortex and the scour process.

Finally, using the recollected data, the temporal behavior, in terms of a non-dimensional parameter, with the large spatial scale of scour formulation and the spatial distribution of the sands slides were correlated.

1.5. Structure of the thesis

The present work contains a total of five chapters. Chapter 1 describes the general problem, working hypothesis, objectives and working methodology. Chapter 2 presents a characterization of the horseshoe vortex system, as well as a large spatial scale formulation of the scour process. Chapter 3 describes the experimental facility, measuring and data processing techniques. Chapter 4 presents the results, including a spatial and temporal analysis of sand slides. Finally Chapter 5 highlights the main conclusions from the obtained results.

CHAPTER 2. STATE OF THE ART REVIEW

2.1. Introduction

This chapter defines and introduces the pioneer researches about the characterization of the horseshoe vortex system (HSV). The characterization includes experiment conditions, typically denoted by the Reynolds number Re_D based on the diameter of the obstacle and the bulk approach velocity. The flow field topology in term of the number of vortex and their behavior, both on flat and scoured bed, are necessary to understand how this complex flow field works. Finally, a large spatial scale formulation of the scouring process is presented.

2.2. The horseshoe vortex system dynamic

The adverse pressure gradient induced by a surface-mounted obstacle in a turbulent boundary layer causes the approaching flow to separate and form a dynamically rich horseshoe vortex system (HSV) in the junction of the obstacle with the wall (Dargahi, 1989; Devenport and Simpson, 1990; Paik *et al.*, 2007). The HVS was first studied experimentally by Dargahi (1989) and by Devenport and Simpson (1990). These pioneer studies revealed its main features and rich dynamics. Dargahi (1989) conducted experiments with Re_D between $6*10^3$ and $6.5*10^4$, and described the quasi-periodic shedding of horseshoe vortices. In same research, 2 to 9 vortices were observed at different instants, where the processes of formation, amalgamation, merging, and dissipation of the leading two main vortices was described. Shedding frequencies varied between 0.1 and 2 Hz at $Re_D=3.9*10^4$. A first topology of the time-averaged flow field was deduced. Devenport and Simpson (1990) studied the HVS dynamics at a NACA wing profile with a 3D laser anemometer for a high Reynolds number, $Re_D=1.15*10^5$, flow. A very similar HVS to that observed at circular cylinders was described. Remarkably, Devenport and Simpson (1990) showed the bimodal distribution of the velocities in the vicinity of the main horseshoe vortex and near the wall. The first mode, the zero-flow mode, was observed during approximately 70% of the time, and the second mode, the backflow mode, was observed in the 30%. The time elapsed between the zero-flow and backflow modes was about 0.011 to 0.026 s. The alternation

between the modes was linked to the enhanced wall shear stress near the wall. Paik *et al.* (2007) performed detached eddy simulations of the flow field in Davenport & Simpson's experiment. The simulated flow field showed the presence of hairpin vortices wrapping around the main horseshoe vortex during the occurrence of the backflow mode, which were responsibilized for destabilizing the horseshoe vortex and triggering the alternation to the zero-flow mode. Escauriaza and Sotiropoulus (2011) performed two Detached Eddy Simulations (DES) of the flow field around a circular cylinder with $Re_D = 2*10^4$ and $3.9*10^4$, the latter corresponding to one of Dargahi's experiment. Significant differences were found in the instantaneous flow fields with different Re_D. In the simulation of the case with low Re_D, 4 or 5 vortices were observed, which were shed periodically at a frequency of f = 0.43 Hz. In the simulation of the case with high Re_D, only 2 quasi periodic vortices with f between 0.17 to 0.3 Hz were observed. The simulations confirmed the appearance of hairpin vortices wrapping around the main horseshoe vortex as the destabilizing mechanism of the backflow mode. Apsilidis *et al.* (2015) conducted Particle Image Velocimetry (PIV) measurements for $Re_D = 2.9*10^4$, $4.7*10^4$, $12.3*10^4$. They identified a third mode, the intermediate mode, which was described as a weaker zero-flow mode. The backflow, intermediate, and zero-flow modes were observed during 41.5, 33.8, and 11.2% at the low Re_D experiment, 31.7, 36.1, and 32.3% at the middle Re_D experiment, and 31.3, 39.6, and 19.3% at the high Re_D experiment. The rest of the time, a disorganized flow field was observed which could not be linked to any of the previously identified modes. Further, Chen *et al.* (2017) observed that the intermediate mode reported by Apsilidis *et al.* (2015) was linked to the appearance of a junction vortex. Schanderl *et al.* (2016, 2017a, 2017b) conducted highly resolved Large Eddy Simulations (LES) of the flow field around a cylinder with $Re_D = 3.9*10^4$, simulating the flow field in close vicinity to the wall. The numerical results revealed the features of the near-wall jet-like structure occurring in the separated region, the main contributor to the turbulent kinetic energy budget, as well as to the wall shear stresses. In time average, the bed shear stress amplification due to the occurrence of the horseshoe vortex by a factor of 3. Kirkil *et al.* (2008) performed the first LES of the flow around a cylinder in an equilibrium scour hole, showing that the flow properties are basically coincident with those observed at a cylinder on a flat bed. Link *et al.* (2013) confirmed that flow at the symmetry plane in front of the cylinder exhibits the same dynamics described in previous experiments and simulations of flows past obstacles in flat beds.

2.3. Large spatial scale of analysis: Dimensionless Effective Flow Work (DFW)

At a larger spatial scale of analysis, Pizarro *et al.* (2017) proposed a formulation for the work by the flow on the sediment bed around a cylinder:

$$W^* = {F_d}^3 U^* = {F_d}^3 \frac{u_{ef} t}{(D^2/2d_s)} = \int_0^{t_{end}} {F_d}^3 \frac{u_{ef}}{(D^2/2d_s)} dt, \quad (2.1)$$

where $F_d = u_{ef}/\sqrt{\rho' g d_s}$ is the effective densimetric Froude number, $u_{ef} = u - u_{c,s}$ is the effective velocity, $u_{c,s}$ is the threshold velocity for scour inception, $\rho' = (\rho_s - \rho)/\rho$ is the relative density, d_s is the sediment particle diameter, D is the pier diameter, and t is the time. Further, Link *et al.* (2017) proposed a simple mathematical model for the estimation of the time-dependent scour depth as a function of the dimensionless effective flow work:

$$Z^* = c_1\left(1 - e^{-c_2 W^{*c_3}}\right), \quad (2.2)$$

where c_1, c_2 and c_3 are model parameters. Moreover, Link *et al.* (2018) showed that similitude of the normalized scour depth $Z^* = z/(D^2/2d_s)$ is given for identic values of W* and the dimensionless grain diameter $D^* = (\rho' g/\upsilon^2)^{1/3} d_s$ in prototype and model. Note that the velocities in Eq. (2.1) can be replaced by the corresponding bed shear stresses, to obtain a formulation in terms of the Shields parameter instead of the densimetric Froude number (see e.g. Oliveto and Hager, 2002). Thus, the dimensionless effective flow work W* is consistent with the enhanced wall stresses caused by the horseshoe vortex. In this work, an additional concept is used, the effective work flow rate, $\partial Z^*/\partial W^*$, which describes the work W* needed to deepen the scour hole depth, Z*, in a given amount.

2.4. Conclusions

Even though the HSV has been extensively studied, the phenomenon is highly complex. Typically, the dimensionless parameter of Reynolds number is used to characterize the

experiments in junction flows. The number of vortices depends on this number, but in the time-averaged sense, two large-scale vortices dominate the flow field topology at a plane in front of the obstacle. Statistical analysis in the vicinity of the main vortex and near the wall exhibited a bimodal velocity distribution, associated to the presence of two states, backflow and zeroflow. The backflow mode corresponds to the existence of a well-organized horseshoe vortex, and the zeroflow mode corresponds to the dissipation of this well-organized vortex due to hairpin vortices wrap around it and retreat the horseshoe vortex toward the obstacle. The interplay between these two modes produces high bed shear stresses. In addition, latest research has found the presence of a third mode called intermediate, with features between the other two mentioned. The main contributor of the wall shear stresses is the near-wall jet-like structure, which can also be described in term of the backflow and zeroflow modes. Finally, numerical simulations reveal that most of the flow properties observed in flat bed were also observed in the case of scoured bed.

As a tool of analysis, a formulation for the estimation of the time-dependent scour depth in function of the dimensionless effective flow work was presented, where the dimensionless effective flow work W* is consistent with the enhanced wall stresses caused by the horseshoe vortex. The effective work flow rate $\partial Z^*/\partial W^*$ was defined, which describes the work given by the flow to obtain a determined scour depth. This concept must include some implicit features of the horseshoe vortex behavior at determined scour depth stage.

The quasi-periodic vortex shedding is related with the periodicity of the interplay between backflow and zeroflow modes. The interplay produces variability in the bed shear stresses, triggering different sediment transport mechanisms, in special, when bed shear stresses decreased, which is one of the main factors which causes sand slides. The zeroflow flow mode is linked with the decreasing shear stresses.

The described laboratory experiments and numerical simulations gives us some clues to understand how the complex flow flied works, as well as the mechanisms which trigger the sediment transport and its behavior.

CHAPTER 3. MATERIALS AND METHODS

3.1. Introduction

This chapter describes the physical model used to carry out scour experiments and characterize the sand slides in front of the pier. Additionally, the measuring techniques used to measure scour depths and record sand slides in front of the pier, the analysis techniques necessary to extract features from the data, and the experimental series conducted under specific hydraulic conditions are also explained.

3.2. Experimental setup

Experiments were carried out in a rectangular laboratory flume of 26 m long, 1.5 m wide, and 0.74 m deep located at the Hydraulic Engineering Laboratory of the University of Concepción. Figure 3.1 shows a scheme of the experimental installation.

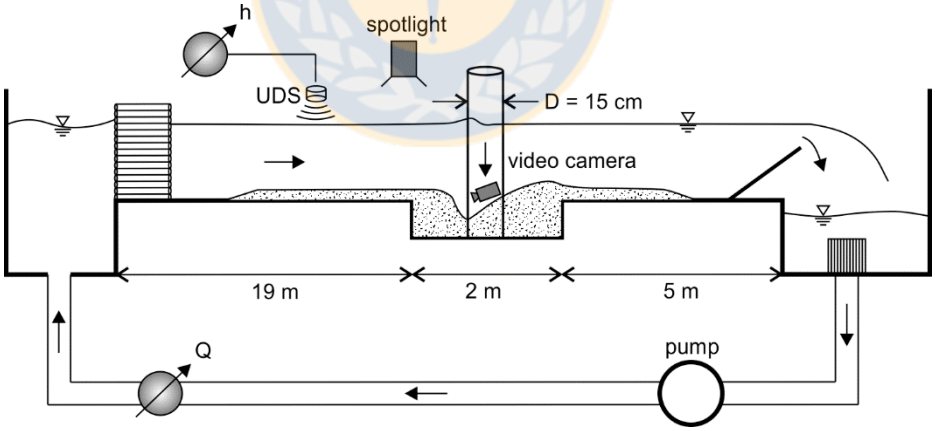

Figure 3.1 Scheme of the experimental installation

A honeycomb matrix aligned the incoming flow after the inlet, and a fully turbulent boundary layer developed. 20 m downstream from the inlet a sediment recess of 2 m in length, and 0.3 m in depth was build. A vertical plexiglass cylinder of 0.15 m in diameter was mounted in the center of the sediment-recess. The discharge Q was measured with an orifice plate device installed in

the recirculation system with a precision of ±1%. The flow depth h was controlled by adjusting a tailgate at the end of the flume and measured with an ultrasonic distance sensor (UDS) with a precision of ± 0.1 mm. The bulk channel velocity was calculated as U=Q/(bh), where b is the flume width. In the experiments, fine uniform sand was used as bed material. The diameter of the grains that passed 50% in weight was d_{50} = 0.36 mm. The critical velocity for inception of sediment motion at the undisturbed, plane bed was measured with an ADV in preliminary experimental runs. It corresponded well with the Shields criterion. The main sediment properties are summarized in the Table 3.1.

Table 3.1 Properties of the bed material

Property	**Value**
Particle density ρ_s (kg m^{-3})	2650
Repose angle ϕ (°)	33
Grain diameter d_{50} (mm)	0.36
Standard deviation of sediment size distribution σ_g (-)	1.40
Dimensionless grain diameter D* (-)	9.11
Critical velocity U_c (m s^{-1})	0.31

3.3. Measuring techniques

3.3.1. Scour measuring

Scour depths around the cylinder were measured with a laser distance sensor (LDS) with an accuracy of ±0.40 mm and a sampling frequency of 70 Hz. The sensor was located inside the plexiglass cylinder and was carefully aligned in horizontal and radial direction to avoid any refraction in the cylinder wall as described in detail by Link *et al.* (2013). The LDS was driven with a step motor in the vertical axis with a precision of ±1/50 mm. The measuring frequency decreased with time as the scour rate decreased towards equilibrium.

3.3.2. Digital image processing

Sand slides were recorded with a CMOS camera placed inside the pier. The camera was mounted on the same positioning system used for the LDS. The camera was inclined 20 degrees down to improve the visualization of sand slides. Images of the upstream portion of the scour hole were recorded. They covering a view of 65° of the total scoured surface. A chessboard-like calibration plate was located in the scoured hole. The position of this plate was carefully selected to follow the shape of the scoured hole measured with the LDS at different stages. Images of this plate were used to assess the optical deformations induced by the transparent cylinder, lens, and the viewing angle of the camera. The images had a resolution of 1280 x 720 pixels and were acquired with a frequency of 30 Hz using an 8 bit intensity scale (values range from 0 to 2^8 - 1). The recording area was illuminated by means of a diffused spotlight, which was located upstream to avoid the presence of high-intensities of light over the bed. The sediment was characterised by a homogeneous color. The zone where the slides occurred received less light than the sand located at the upper part, thus the events were easily identified by a change of intensity.

3.4. Processing and analysis techniques

3.4.1. Digital image processing for characterization of sand slides

Digital image processing techniques were applied to the recorded videos of the sand slides occurring at the upstream portion of the scour holes to identify the slide events, and to obtain the frequency and magnitude of the sand slides. The digital image processing included binarization and filtering. Figure 3.2 illustrates a sequence of the digital image processing.

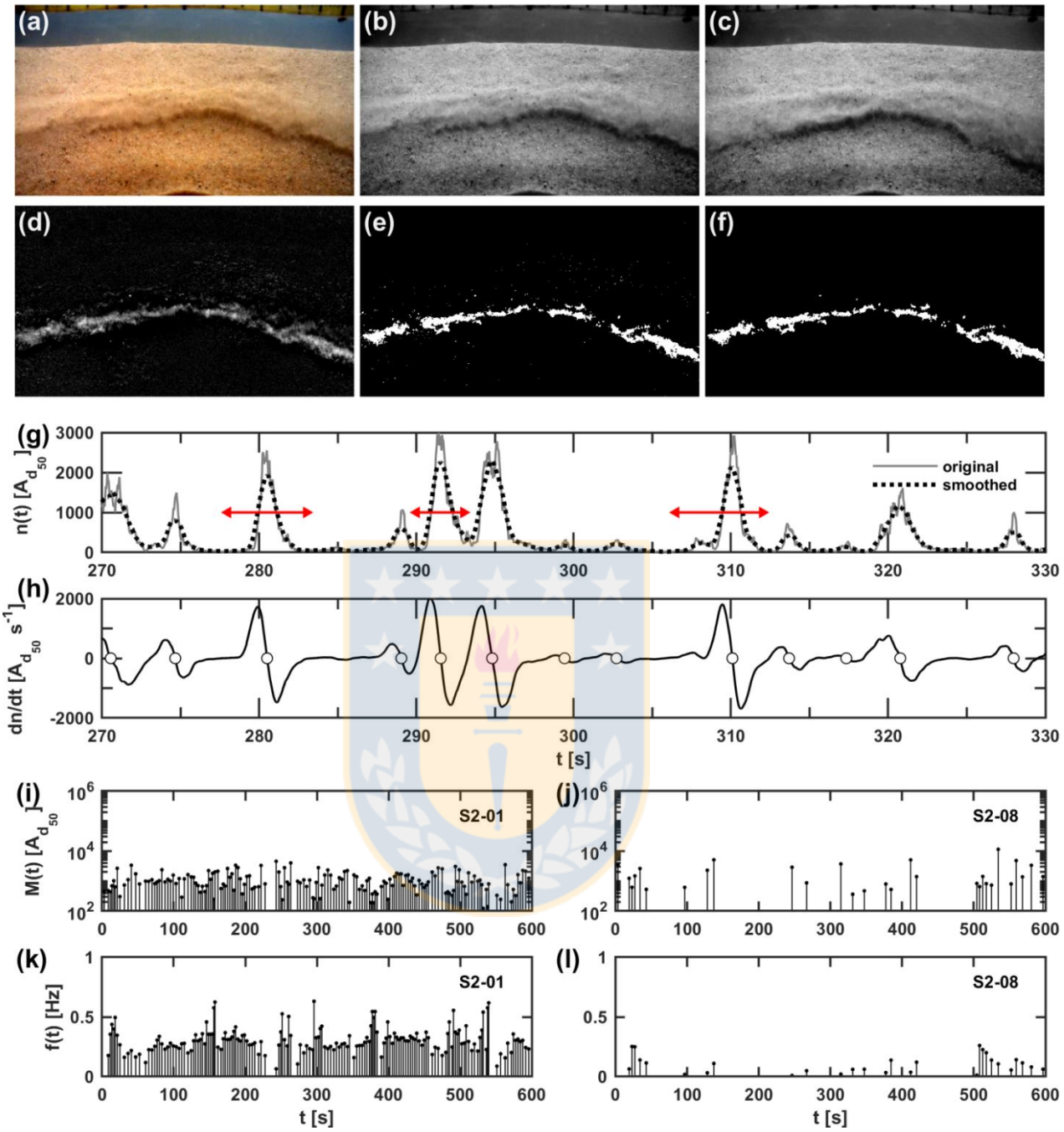

Figure 3.2 Sequence of the image processing: (a) raw image. (b) and (c) consecutive video images in greyscale. (d) result from subtraction of image in (c) from image in (b). (e) binary image with noise. (f) filtered binary image. (g) original time series of events, i. e. sand slides in motion. (h) smoothed time series. Circles represent the detected events and the red arrows show the duration of three events. (i) and (k) show the estimated magnitude and frequency of sand slides at the initial stages of the series S2. (j) and (l) show the estimated magnitude and frequency of sand slides at the final stages of series S2.

Raw video images were transformed from color images to grayscale in order to reduce their size thus facilitating its digital processing. Next, intensities at each pixel in consecutive video images were subtracted as described by Radice *et al.* (2006). A binarization of the resulting image highlighted the image area corresponding to sediment particles in motion. The image binarization was sensitive to the selected threshold value, thus it was carefully and manually determined for each case from the local frame sequences without sand slides. The threshold selection criterion was such that in those frames without sediment motion, the resulting binarized image had intensities near zero. Binary images contained some noise in pixels corresponding to isolated sediment particles in motion that did not pertain to the sand slide, or also to areas with important light reflection due to surface waves. The noise was filter out using the MATLAB function bwareaopen, which removes all connected components (objects) that have fewer than a threshold number of pixels from the binary image. The threshold number was 10 pixels which corresponded to approximately 2 times d_{50}. The conversion from pixel to grain of d_{50} was obtained measuring the darker particles which make contrast with lighter particles on the section where was detected sediment slides, and then as the sediment size distribution was homogeneous, the pixel area measured was associated to an area produced by the projection of a spherical particle of d_{50}, with unit of measurement equal to A_{d50}. After digital image processing, time series of surface in motion n at the front of the scour hole were obtained. Sand slide events occurred at local maximum of the curve. These were identified where $dn/dt = 0$ and $d^2n/dt^2 < 0$. The sand slide magnitude M was computed as the time integral of the surface in motion over the event duration in units of d_{50}. The instant frequency f was computed using the time difference between two consecutive sand slides events, and then the reciprocal of this time value was associated to the last event. Mean sand slides frequency $\bar{f}$, mean sand slides magnitude $\bar{M}$ and standard deviation of sand slides magnitude σ_M were computed. Finally, the scoured volume caused by sand slides ΔV_{ss} during a determined segment of time Δt was estimated by means of $V_{ss} = \bar{f}\bar{M}\Delta t$, where $\bar{f}\,\bar{M}$, describes its scouring rate.

3.4.2. Proper Orthogonal Decomposition

A Proper Orthogonal Decomposition (POD) was performed to the sequence of binarized images to obtain a description of the avalanche dynamics based on a reproducible statistical analysis. The POD is a technique aimed at identifying the optimal set of linear modes, and their associated time coefficient, that contribute the most, from an statistical point of view, to the variance of the signal (Brevis and Garcia-Villalba, 2011, Higham et al, 2018). The technique has been used in the past for the analysis of turbulent velocity fields, for filtering and interpolation of experimental measurements (Higham et al, 2016) and in particular for the analysis of image sequences containing visualisations of the flow dynamics (Brevis and Garcia-Villalba, 2011). The technique was selected, over other modal decomposition techniques, based on the fact that is one of the few synoptical methods offering a ranking criteria that can be directly related to parameters representing the phenomena of interest, in this case the variance of the signal, or in terms of intensities, the occurrence of slide events.

Before performing the POD analysis and due to computational limitations, the resolution of the binarized video images was reduced using a bicubic interpolation method. For time series of 10 and 40 minutes, the scale factor was 2:1 and 5:2, respectively. Additionally, a reduction of the frame rate was performed, using as a reference the Nyquist criteria and an estimated frequency of events given by $\bar{f}+2\sigma_f$. For video durations of 10 and 40 minutes the selected frame rate was 30 and 10 Hz, respectively. Analogously to the Reynolds decomposition, the mean image of each time series was computed and subtracted from the instantaneous frames. The fluctuating time series was used for the POD analysis.

3.5. Experimental series

Three series of experiments with a constant discharge and clear water conditions were performed. In each series, a different flow intensity U/U_c was imposed namely 0.68, 0.78 and 0.84 for series S1, S2, and S3, respectively. The corresponding cylinder Reynolds number Re_D was 31500, 36190 and 39000, and the corresponding Froude numbers, $Fr = U/\sqrt{gh}$, where g is the

gravitational acceleration, was 0.141, 0.162 and 0.175, respectively. The duration of the experiments in series S1, S2, and S3 was 30, 48 and 48 hours with final maximum scour depths equal to 6.0, 12.2 and 16.4 cm, respectively. The scour depth z and the time t were non-dimensionalized using z_{max} = 16.4 cm and t_{max} = 48 h, which correspond for the case with highest flow intensity. The volume of the scour hole V was estimated using the expression proposed by Yanmaz and Altinbilek (1991) for cylindrical piers, and then non-dimensionalized using V_{max} equal to 20711 cm^3, calculated with z_{max}. Sediment slides were recorded at different scour stages. The scour rate, dz/dt, was used as a criteria to set the number of images recorded in each stage, where dz/dt = 0.4 cm/h was the threshold value. In early stages of scour the number of images was 18000 corresponding to 10 minutes of video record, while in intermediate and advanced stages of scour the number of images was 72000 corresponding to 40 minutes of video record. Table 3.2 shows the important parameters of the conducted experiments.

Table 3.2 Experimental series

Image ID	**U/U_c**	**Re_D**	**z/z_{max}**	**t/t_{max}**	**N [images]**
S1-01	0.68	31500	0.32	0.42	69837
S1-02	0.68	31500	0.36	0.54	71972
S2-01	0.78	36190	0.32	0.07	17972
S2-02	0.78	36190	0.36	0.10	17972
S2-03	0.78	36190	0.43	0.17	71972
S2-04	0.78	36190	0.49	0.26	71958
S2-05	0.78	36190	0.55	0.40	71972
S2-06	0.78	36190	0.61	0.56	71972
S2-07	0.78	36190	0.67	0.76	71972
S2-08	0.78	36190	0.73	0.96	71972
S3-01	0.84	39000	0.32	0.02	17972
S3-02	0.84	39000	0.36	0.04	17972
S3-03	0.84	39000	0.43	0.06	17972
S3-04	0.84	39000	0.49	0.10	17972
S3-05	0.84	39000	0.55	0.15	17972
S3-06	0.84	39000	0.61	0.21	71972
S3-07	0.84	39000	0.67	0.28	71957
S3-08	0.84	39000	0.73	0.36	71972
S3-09	0.84	39000	0.79	0.46	71958
S3-10	0.84	39000	0.85	0.53	71957

Figure 3.3 shows the properties of the resulting scour holes in the conducted experiments, namely the scour depth over time, dimensionless flow work over time, scour depth over dimensionless flow work, and scour hole volume over scour depth. As is expected, maximum scour depth increased with the flow intensity, and the erosion rate decreased with time. The discharge Q was constant during all the experimental runs, causing that the work W* transferred from the flow increase in a constant rate. The dimensionless grain diameter D* was the same in the three series, as a result, scour only was controlled by dimensionless effective flow work W* and the three series converge in one tendency. The scoured volume estimated with the formula proposed by Yanmaz and Altinbilek (1991) is function of the sediment diameter d_{50}, pier diameter D and repose angle ϕ; so, there is no difference in the scoured volume at a same scour depth when a different flow intensity was studied.

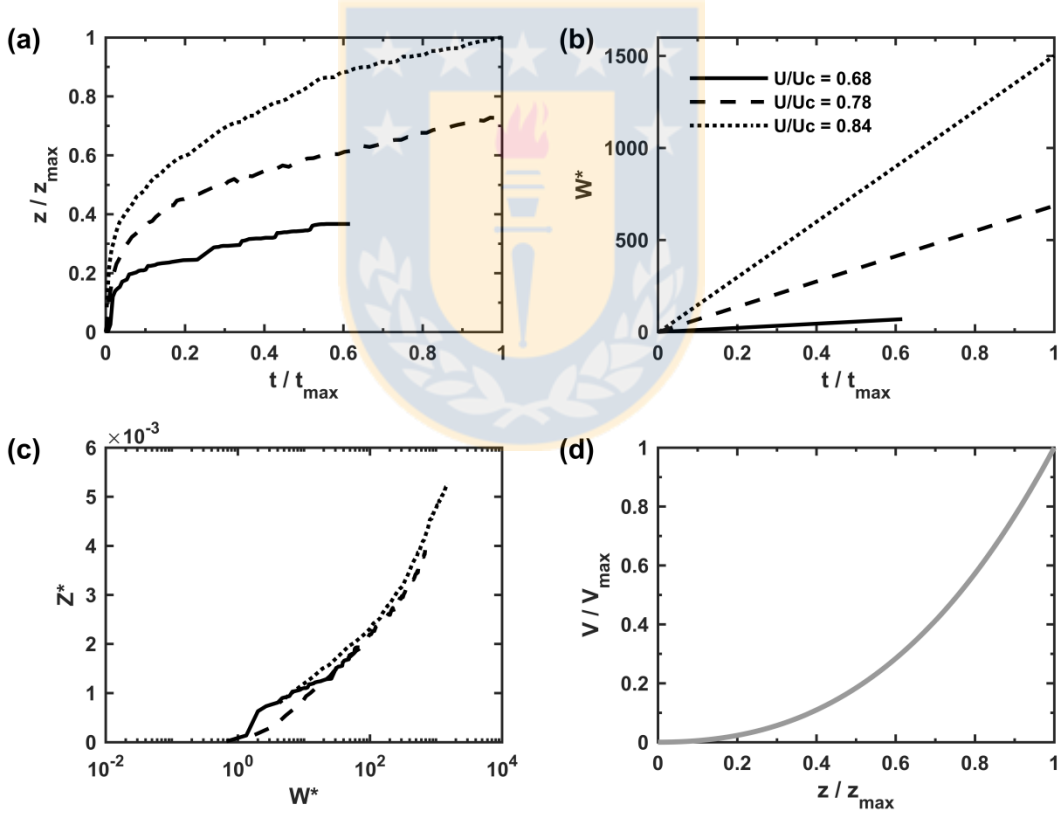

Figure 3.3 Scour depth over time (a), work over time (b), scour depth over work (c), and scour hole volume over scour depth (d).

3.6. Conclusion

The experimental configuration was defined to study sand slides under clear water conditions. A total of three series were selected, where a different flow intensity U/U_c was imposed. The flow intensities were equals to 0.68, 0.78 and 0.84, which caused a notorious difference in the scour depth over time. The flow conditions also varied the Reynolds number R_D, an important parameter to characterize the horseshoe vortex dynamic.

The scour depth was measured with a laser distance sensor, and the sand slides were recorded with a CMOS camera, both located inside the pier to measure in a non-intrusive manner. The processing to identify sand slides from recorded images is summarized in three steps: subtraction, filtering and binarization. The final result corresponds to binary images, where white pixels highlighted the surface with sediment particles in motion. From binary images, some features are extracted, time series which show the presence of events of sand slides and their magnitude in terms of particle of d_{50}, and the spatial distribution in terms of the most important structures in motion. Finally, from time series is estimated a mean frequency that occurs and avalanche and its magnitude.

CHAPTER 4. RESULTS

4.1. Introduction

The results obtained from binary image analysis are introduced. Firstly, sand slides characterization in term of frequency and magnitude is presented. Secondly, a first look of the spatial distribution based on statistical analysis is described. Thirdly, sand slides Strouhal number is defined, and then connected with the dimensionless effective flow work and the characteristic pattern of the spatial distribution. Finally, the scoured volume contribution due to sand slides mechanism is briefly discussed.

4.2. Frequency and magnitude of sand slides

Figure 4.1 shows over normalized scour depth the mean frequency $\bar{f}$, mean magnitude $\bar{M}$ and standard deviation of the magnitude σ_M, as well as the product of magnitude and frequency which expresses the rate of sediment erosion caused by sand slides. In all series mean frequency decreased, and mean magnitude increased with time. The magnitude exhibited an increasing variability with scour depth. The product of the magnitude with the frequency of side slides decreased in time, evidencing a decrease in the erosion caused by sand slides towards equilibrium conditions. Taking a scour depth as a reference, the frequency, the magnitude, as well as their product, increase with flow intensity.

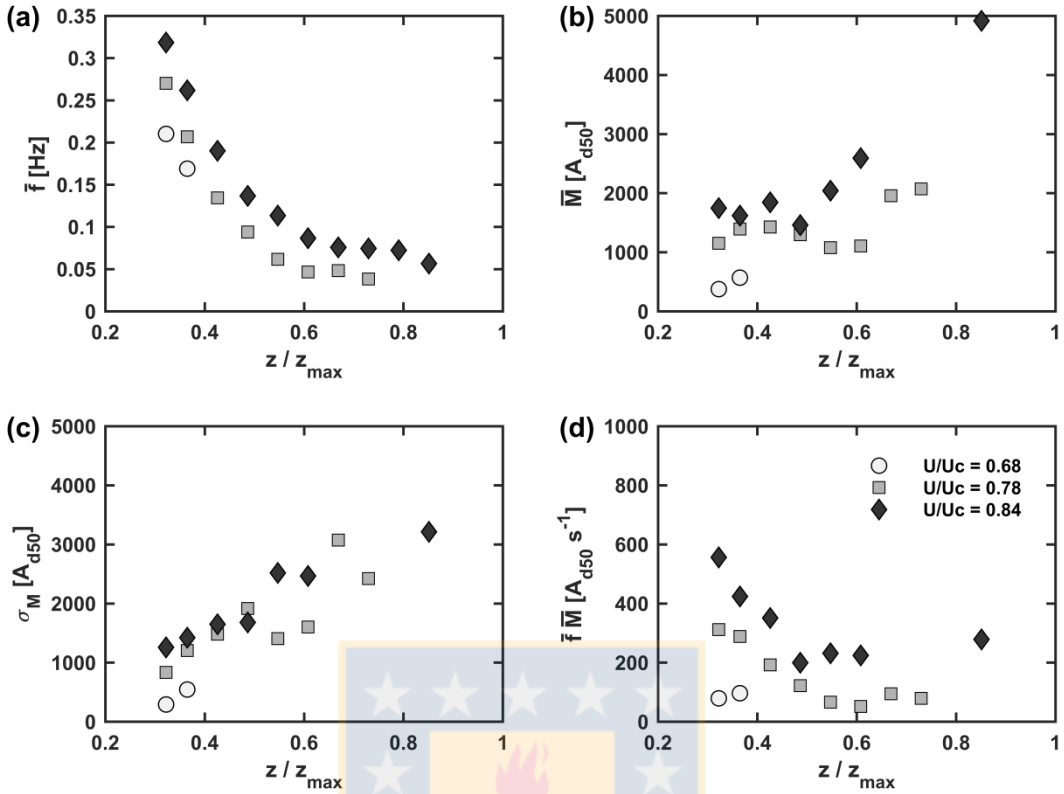

Figure 4.1 Mean frequency of side slides (a), mean magnitude of sand slides (b), standard deviation of the magnitude of sand slides (c), and the product of magnitude and frequency of side slides (d), on normalized scour depth for series S1, S2, and S3.

4.3. Spatial distribution of sand slides

The modes obtained from the POD revealed the characteristic patterns of the spatial distribution of sand slides and their dynamics. As in typical POD results, positive and negative values in the spatial modes correspond to the presence of structures which change magnitude according to the evolution of the time coefficients, while zero values display regions with absence of sand slide activity. Figure 4.2 shows the four most energetic modes for early (S2-01, S3-01), intermediate (S1-01), and advanced (S1-02, S3-08, S2-10) stages of scour.

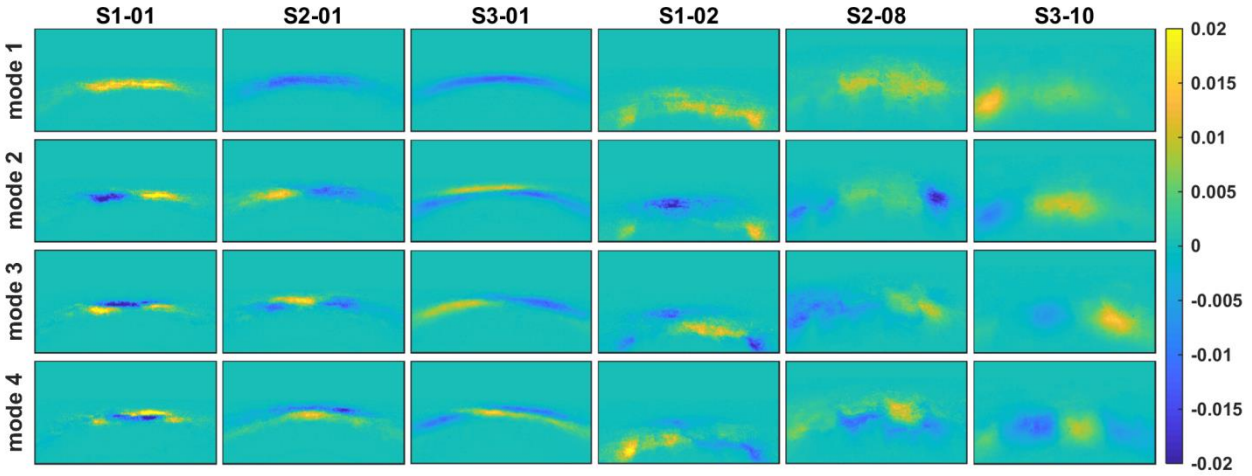

Figure 4.2 Four most energetic modes for early (S2-01, S3-01), intermediate (S1-01), and advanced (S1-02, S3-08, S2-10) stages of scour.

Similar dominant modes are observed in the three experimental series during the different stages of scour experiments. The first four most energetic modes appear in many cases at early and intermediate stages, suggesting that the slide mechanism is independent of the flow intensity. Mode 1 was the same in all experiments, exhibiting a strip shaped surface that emphasizes the area where the activity was detected in the video. A more detailed sediment distribution inside this mode was characterized by modes 2, 3 and 4. The mode 2 showed a strip divided at the center, revealing that a portion of the sliding surface slides before the portion on the other side separated by a brief delay but pertaining to the same event. This pattern was generally the second most energetic. Nevertheless, it was also observed in less energetic rank positions, e.g. in mode 3 for experiment S3-01. The modes 3 and 4 were very similar, showing two stripes grouped one over the other, revealing the slide dynamics in the vertical direction. During advanced stages of scour, dominant modes become less symmetric and spatially irregular. The defined stripe pattern observed at earlier stages disappeared, and the vertical dimension of the displaced surface increased. There were no similar modes and they revealed the presence of more specific kind of sand slides. Typically the first modes described the initial position of the sand slide, and the higher modes revealed the vertical movements. Interestingly, sand slides in experiment S3-10 showed modes with discrete patches of sediment, suggesting the generation of more localized sand slides that cover only the left side, right side or the center of the upstream part of the scour hole.

4.4. Sand slide Strouhal number, dimensionless effective flow work, and sand slide types

Figure 4.3 shows the side slides Strouhal number over the derivative of dimensionless scour respect to the dimensionless flow work, with the corresponding avalanche dominant modes.

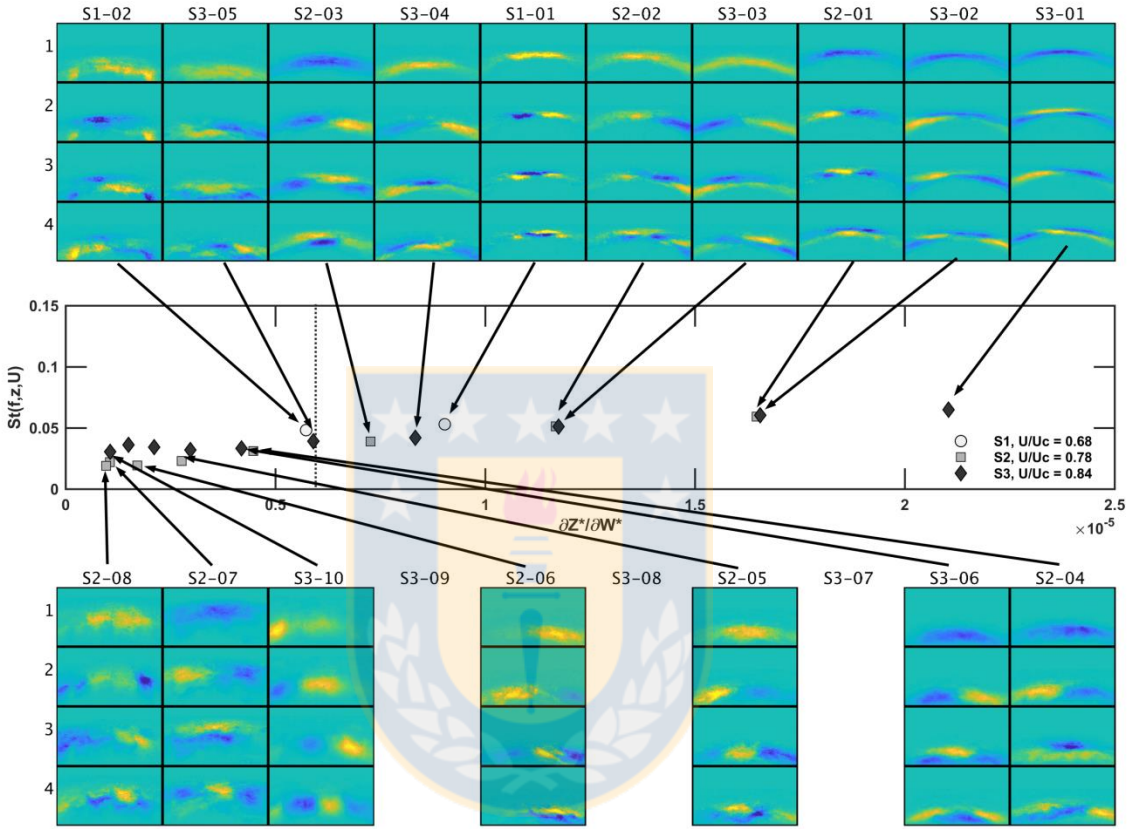

Figure 4.3 Side slides Strouhal number over the derivative of dimensionless scour respect to the dimensionless flow work, with the corresponding avalanche dominant modes.

The side slide Strouhal number was defined as the ratio of the sand slide mean frequency to the flow velocity divided by the scour depth. The sand slide Strouhal number slightly increased in a nearly linear manner with the dimensionless flow work, W* needed to deepen the scour hole depth, Z* in a given amount, $\partial Z^*/\partial W^*$. Importantly, results of all experiments collapsed into one tendency. Noticeably, sand slides of Type I occurred for low values of $\partial Z^*/\partial W^*$, i.e.: during the final stage of scour, while sand slides of Type II occurred for high values of $\partial Z^*/\partial W^*$, i.e. during initial and intermediate stages of scour. The transition between the two side slides types was estimated around $\partial Z^*/\partial W^*$ equal to $0.6*10^{-5}$.

4.5. Contribution of sand slides to scour

Figure 4.4 shows the percentage of scoured volume due to avalanches over normalized scour depth.

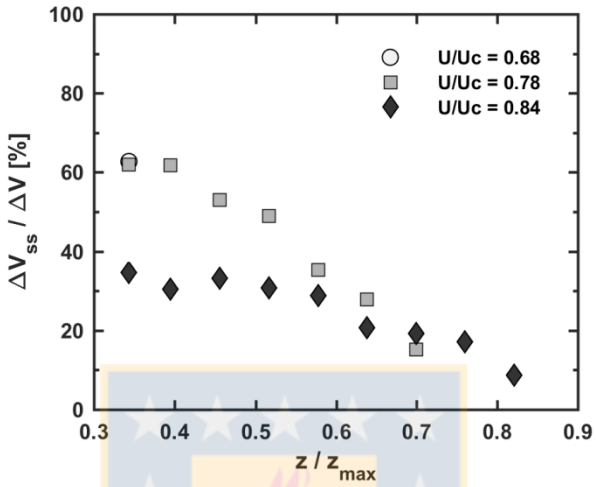

Figure 4.4 Percentage of sand slide volume ΔVss with respect to the scoured volume ΔV.

The contribution of side slides to the total scoured volume $\Delta V_{ss}/\Delta V$ was computed between the scour depths showed in Table 3.2, assuming that slides have a thickness of one sediment grain diameter, d_{50}. Moreover, the contribution was computed from the images that recorded side slides at the upstream front of the scour hole, with an angle of 65°. Overall, the contribution of side slides to scour is high, varying between 37 and 63% at the beginning of scouring, and decreasing towards zero in the equilibrium scour phase. The side slides contribution to scour was smaller in series S3 during initial and intermediate scour stages. Curiously, series S3 has the highest flow intensity of 0.84. This is attributed to the increasing turbulence with flow intensity (e.g. Escauriaza and Sotiropoulus, 2011). Under higher flow intensities other scour mechanisms different than side slides, such as particle entrainment into suspension due to sweeps and ejections by hairpin vortices, appear to be of higher relative importance for scour. In the downstream portion of the scour hole, different scouring mechanisms are observed, such as advection of entrained particles, ejections due to flow separation. Especially in the cylinder wake, tornado-like wake vortices are able to mobilize small sediments, although a deposition zone where a dune-like bedform develops has been described (Oliveto and Hager, 2014).

4.6. Conclusions

Results showed that the mean frequency decreased and the mean magnitude increased with time. The flow intensity increased both mean frequency and mean magnitude of the sand slides. The spatial distribution characterized by POD showed similar dominant modes at early and intermediate stages of scouring in the three flow intensities studied. The result is interesting because suggest that the mechanism which produces the slide is the same independent of the flow intensity. For advanced stages, POD modes showed more disorganized structures.

Sand slide Strouhal number, defined as the ratio of the sand slide mean frequency to the flow velocity divided by the scour depth, correlated with the dimensionless flow work needed to deepen the scour hole depth, $\partial Z^*/\partial W^*$, suggesting that the integral scale is close related to the sediment motion responsible for an important part of the scour. Additionally, two kinds of sand slides were identified along this tendency, Type I for high values of $\partial Z^*/\partial W^*$, while Type II for low values of $\partial Z^*/\partial W^*$.

Finally, the contribution of side slides to scour varied between 37 and 63% at the beginning of scouring, and decreased towards the equilibrium scour phase.

CHAPTER 5. CONCLUSIONS

The sand slides in the front of a scour hole around a cylinder in a sand bed were investigated experimentally in a large laboratory flume, through videoing and digital image processing. Three experimental series with different constant discharges were conducted until advanced stages of scour. Sand slides were recorded in a non-intrusive manner using a video camera placed inside of the pier.

In time, sand slides occurred intermittently in an aperiodic manner and with different magnitudes resembling the behavior of the horseshoe vortex typically forming in junction flows. Mean frequency of sand slides decreased, and mean magnitude of sand slides increased with time. The product of both decreased in time, evidencing a decrease in the erosion caused by sand slides towards equilibrium conditions. At a same scour depth, flow intensity increased the mean frequency and mean magnitude.

Two types of sand slides were identified through a Proper Orthogonal Decomposition: Type I is a short and long advancing sand slide, while Type II is an elongated and short advancing sand slide.

The sand slide Strouhal number defined as the ratio of the sand slide average frequency by the scour depth to the flow velocity correlated with the derivative of scour depth respect to the dimensionless flow work. Remarkably, sand slides of Type I occurred for low values of $\partial Z^*/\partial W^*$, while sand slides of Type II occurred for high values of $\partial Z^*/\partial W^*$.

Sand slides contributed to produce about 40 to 60% of the scoured volume, depending on the flow intensity. The obtained results clearly show the need to improve current numerical models for physically based simulations of the scour mechanisms.

REFERENCES

Apsilidis, N., P. Diplas, C.L. Dancey and P. Bouratsis (2015) Time-resolved flow dynamics and Reynolds number effects at a wall–cylinder junction. **Journal of Fluid Mechanics. 776.** 475-511.

Apsilidis, N., P. Diplas, C.L. Dancey and P. Bouratsis (2016) Effects of wall roughness on turbulent junction flow characteristics. **Experiments in Fluids. 57.** 12.

Brandimarte, L., P. Paron and G. Di Baldassarre (2012) Bridge pier scour: A review of processes, measurements and estimates. **Environmental Engineering and Management Journal. 11(5).** 975-989.

Brevis, W., and M. García-Villalba (2011) Shallow-flow visualization analysis by proper orthogonal decomposition. **Journal of Hydraulic Research. 49(5).** 586-594.

Chen, Q., M. Qi, Q. Zhong, D. Li (2017) Experimental study on the multimodal dynamics of the turbulent horseshoe vortex system around a circular cylinder. **Physics of Fluids. 29.** 015106.

Dargahi, .B (1989) The turbulent flow field around a circular cylinder. **Experiments in Fluids. 8(1-2).** 1-12.

Devenport, W.J., and R.L. Simpson (1990) Time-dependent and time-averaged turbulence structure near the nose of a wing-body junction. **Journal of Fluid Mechanics. 210.** 23-55.

Escauriaza, C., and F. Sotiropoulos (2011) Reynolds number effects on the coherent dynamics of the turbulent horseshoe vortex system. **Flow, Turbulence and Combustion. 86.** 231–262.

Higham, J.E., W. Brevis and C.J. Keylock (2016) A rapid non-iterative proper orthogonal decomposition based outlier detection and correction for PIV data. **Measurement Science and Technology. 27(12).** 125303.

Higham, J.E., W. Brevis and C.J. Keylock (2018) Implications of the selection of a particular modal decomposition technique for the analysis of shallow flows. **Journal of Hydraulic Research. 56(6).** 796-805.

Kirkil, G., G. Constaninescu and R. Ettema (2008) Coherent structures in the flow field around a circular cylinder with scour hole. **Journal of Hydraulic Engineering. 134(5).** 572-587.

Link, O., C. González, M. Maldonado and C. Escauriaza (2013) Coherent structure dynamics and sediment particle motion around a cylindrical pier in developing scour holes. **Acta Geophysica. 60(6).** 1689-1719.

Link, O., C. Castillo, A. Pizarro, A. Rojas, B. Ettmer, C. Escauriaza and S. Manfreda (2017) A model of bridge pier scour during flood waves. **Journal of Hydraulic Research. 55(3).** 310-323.

Link, O., S. Henríquez and B. Ettmer (2018) Physical scale modelling of scour around bridge piers. **Journal of Hydraulic Research**.

Oliveto, G., and W. Hager (2002) Temporal evolution of clear-water pier and abutment scour. **Journal of Hydraulic Engineering. 128(9).** 811-820.

Oliveto, G., and W. Hager (2014) Morphological evolution of dune-like bed forms generated by bridge scour. **Journal of Hydraulic Engineering. 140(5).** 06014009.

Paik, J., C. Escauriaza and F. Sotiropoulos (2007) On the bimodal dynamics of the turbulent horseshoe vortex system in a wing-body junction. **Physics of Fluids. 19.** 115104.

Pizarro, A., B. Ettmer, S. Manfreda, A. Rojas and O. Link (2017) Dimensionless effective flow work for estimation of pier scour caused by flood waves. **Journal of Hydraulic Engineering. 143(7).** 06017006.

Radice, A., S. Malavasi and F. Ballio (2006) Solid transport measurements through image processing. **Experiments in Fluids. 41.** 721-734.

Schanderl, W., and M. Manhart (2016) Reliability of wall shear stress estimations of the flow around a wall-mounted cylinder. **Computers & Fluids. 128.** 16-29.

Schanderl, W., U. Jenssen, C. Strobl and M. Manhart (2017a) The structure and budget of turbulent kinetic energy in front of a wall-mounted cylinder. **Journal of Fluid Mechanics. 827.** 285-321.

Schanderl, W., U. Jenssen and M. Manhart (2017b) Near-wall stress balance in front of a wall-mounted cylinder. **Flow, Turbulence and Combustion. 99.** 665-684.

Yammaz, A.M., and H.D. Altinbilek (1991) Study of time-dependent local scour around bridge piers. **Journal of Hydraulic Engineering. 117(10).** 1247-1268.